Opto-Electronics Review 30 (2022) e141950

POLISH ACADEMY OF SCIENCES

Opto-Electronics Review

journal homepage: https://journals.pan.pl/opelre

Hybrid FSO/mmWave wireless system: A plausible solution for 5G backhaul applications

Isanaka Lakshmi Priya*, Murugappa Meenakshi

Department of Electronics and Communication, Anna University, Guindy, Chennai 600025, India

Article info

Article history:
Received 16 May 2022
Received in revised form 21 Jun. 2021
Accepted 21 Jun. 2022
Available on-line 22 Jul. 2022

Keywords:
Millimeter wave communication; free space optics; carrier availability; backhaul; hybrid wireless system; terahertz communication.

Abstract

The explosive rise of wireless services necessitates a network connection with high bandwidth, high performance, low mistakes, and adequate channel capacity. Individual mobile users, as well as residential and business clusters are increasingly using the internet and multimedia services, resulting in massive increases in the internet traffic demand. Over the past decade, internet traffic has grown significantly faster than Moore's law predicted. The current system is facing significant radio frequency spectrum congestion and is unable to successfully transmit growing amounts of (available) data to end users while keeping acceptable delay values in mind. Free space optics is a viable alternative to the current radio frequency technology. This technology has a few advantages, including fast data speeds, unrestricted bandwidth, and excellent security. Since free space optics is invisible to traffic type and data protocol, it may be quickly reliably and profitably integrated into an existing access network. Despite the undeniable benefits of free space optics technology under excellent channel conditions and its wide range of applications, its broad use is hampered by its low link dependability, especially over long distances, caused by atmospheric turbulence-induced decay and weather sensitivity. The best plausible solution is to establish a secondary channel link in the GHz frequency range that works in tandem with the primary free space optics link. A hybrid system that combines free space optics and millimeter wave technologies in this research is presented. The combined system offers a definitive backhaul maintenance, by drastically improving the link range and service availability.

1. Introduction

The wireless communication dilemma of offering uninterrupted support to the ever-increasing number of end users, creating new services, enhancing existing services, and sharing congested spectrum bands is the fundamental motivation behind the search for the state-of-art and scalable technology. Due to the natural growth of computer and telecommunications technology, every new generation of cellular innovation has a life cycle of a decade or less. The capacity of 5G wireless networks is predicted to increase a thousandfold with connections for at least 100 billion devices and a 10 Gbps individual user experience with incredibly low latency and response times. These networks have been deployed since 2020 with a peak projected in 2030. In general, 5G technology is projected to provide users with an immersive experience (data speeds approaching 10 Gbps), enable ultra-high-definition video, virtual reality apps, and mobile cloud services. 5G networks are supposed to have zero latency and extremely low response and switching times (milliseconds), while keeping energy consumption as low as possible [1, 2]. The requirements of 20 Gbps peak data rate and 1 millisecond latency present significant engineering challenges in the design of 5G cellular systems. For a vast majority, fibre optical communications are the primary technology used for backhaul support. Free space optics (FSO) is an inherently low-latency technology with effectively no delay between packets being transmitted and received at the other end, except for the line of sight (LoS) propagation delay. The speed of light through air is approximately 40% higher than in optical fibres. This equates to a 40% reduction in latency values.

---

*Corresponding author at: priyaisanaka@gmail.com

https://doi.org/10.24425/opelre.2022.141950
1896-3757/ Association of Polish Electrical Engineers (SEP) and Polish Academic of Sciences (PAS). Published by PAS

Use of the millimeter wave (mmWave) bands above 10 GHz, where vast quantities of spectrum are available, makes mmWaves a promising 5G candidate that may be able to rise to the occasion [3, 4].

5G is expected to provide customers with an immersive experience (with rates surpassing 10 Gbps), as well as super high-definition video, virtual reality apps, and mobile cloud services. One such 5G enabling technology that uses alternate spectral region to provide fronthaul services is an optical wireless communication (OWC) [5, 6]. The authors are primarily interested in the OWC technology that is best suited for outdoor terrestrial communications, often known as FSO links [7]. The FSO system has piqued the interest of entrepreneurs all over the world, as it has shown to be one of the most effective last-mile communication solutions in high-traffic regions. It has emerged as a more viable option to radio frequency (RF) technology for a communication network implementation. Despite the widespread existence of RF wireless networks capable of supporting data speeds of several hundred megabits per second, the massive growth in data traffic, range limits, and limited accessible bandwidth have created significant challenges for communication utilizing this technology. Because of its large bandwidth, FSO technology may quickly replace RF technology. FSO communication appears to be an excellent candidate for 5G communication because of its license-free bands, resilience, high data rate transfers, good security, and low signal interference. FSO is a LoS method that transfers data using light travelling in open space. With a minimal system complexity, the connection provides weather. Despite numerous benefits, the link availability under varying climatic circumstances is a major source of worry. Because these linkages are largely weather-dependent, signal attenuation increases under certain conditions, lowering link efficiency.

Different atmospheric conditions, including snow, fog, and rain, scatter and absorb the transmitted signal resulting in a significant signal attenuation before it reaches the receiver. The fundamental obstacle in establishing an overland communication link centred on FSO technology is preserving LoS between transmitter and receiver [8]. The range and capacity of wireless channels are severely constrained due to a signal attenuation induced by atmospheric conditions. The atmospheric attenuation in clear weather ranges from 0.2 dB/km in exceptional sunny weather. Conditions such as heavy snow and thick and heavy fog, on the other hand, dramatically increase attenuation to approximately 350 dB/km, limiting the link capability. The dominance of atmospheric attenuation on link performance is a major impediment to the acceptance of FSO technology as a service provider for end users, as it is highly difficult to achieve carrier-class availability. In order to ensure higher availability while not compromising on data rates, using a GHz range link parallel to the FSO link guarantees a nearly flawless setup [9, 10].

A secondary RF connection is the first and most typical hybrid route that is explored as a backup to the primary FSO link. Several factors such as non-dependency on atmospheric effects, non-LoS, and ease of implementation and cost (already existing) make it a highly valued choice for the secondary link. When considering a technology for commercial viability, the hybrid architecture should be able to satisfy the stringent requirements of a 5G fronthaul network. In general, the data rates offered by RF links are much lower in comparison to the rates offered by the FSO link. However, mmWave technology is a great contender as they exist close to optical frequencies in the electromagnetic (EM) spectrum. They have comparable propagation properties, and because of their enhanced carrier frequencies, both spectral bands provide greatly expanded transmission bandwidths which is one of the driving factors for their introduction into the 5G arena [11].

The frequency range of mmWave frequencies is from 30 GHz to 300 GHz, with a wavelength ranging from 10 mm to 1 mm. At mmWave frequencies, the radio spectrum is still underused, and an additional bandwidth is available. Due to the obvious limited range and very small beam widths, mmWave frequencies provide superior security and privacy. At mmWave frequencies, the spatial resolution is improved because the tiny wavelength allows for the creation of compact antennas with a narrow beam width. At mmWave frequencies, the physical dimensions of antennas shrink to the point where sophisticated antenna arrays may be built. The combined deployment of FSO/mmWave could ensure extremely resilient wireless-based fronthaul networks under various atmospheric and weather conditions. By considering FSO as the fundamental technology, the spectrum scarcity and interference issues in the radio wireless-based fronthaul/backhaul networks can be combated. FSO could also be seamlessly integrated with optical fibres to form an all-optical low-latency and high-capacity backhaul link. The proposed hybrid system combines the extended range of the FSO link with the capacity and availability of mmWave links. This hybrid system is appropriate for mobile platforms due to its potentially large link capacities [12].

2. FSO channel model

Absorption, scattering, turbulence, and precipitation all impact the attenuation of an optical signal as it travels through the atmospheric channel. Presence of aerosols, dust, smoke, and particles of various sizes contributes significantly to the decrease in signal strength. Figure 1 is a holistic summary of all the atmospheric attenuation contributors.

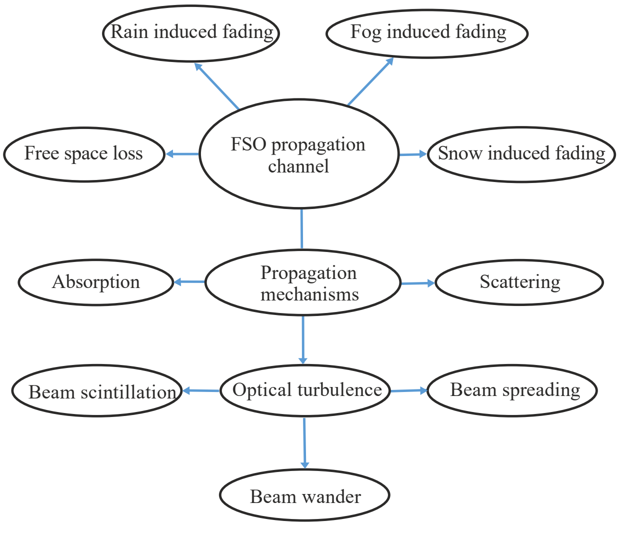

Fig. 1. FSO channel characteristics.

Equation (1) is a mathematical model of the atmospheric channel.

$$y(t) = \gamma\{h(t)x(t)\} + n(t). \tag{1}$$

In the above equation, $y(t)$ is the received optical signal, $h(t)$ is the channel turbulence model, γ is the channel attenuation (dB/km), $x(t)$ is the transmitted optical signal, and $n(t)$ is the noise signal. The attenuation parameter γ includes the effects of absorption, scattering, fog, rain, and snow-induced fading. The channel turbulence para-meter $h(t)$ takes into account the effects of scintillation.

Along with affecting signal strength, certain environmental conditions such as wind can cause building movements and these effects can disrupt the transmitter and receiver alignment. To mitigate these effects, FSO systems use two approaches. First, a wider beam divergence angle can be used initially. Second, active tracking systems can be used to keep beam aligned. Another problem for FSO communication links is scintillation. Temperature of separate air pockets is affected by heated air ascending from the base or roofs. Therefore, the refractive index changes over time as it travels through the connection causing scintillations in the beam. The receiver detects these scintillations as a power fluctuation [13, 14].

Absorption and scattering processes are major contributors to loss in the atmospheric channel. The interaction of photons travelling through the atmosphere with molecules existing along their path results in absorption, scattering, or LoS. The process of absorption is wavelength-dependant [15, 16]. Some photons are destroyed, and their energy transformed to heat, while others are scattered owing to particle components. Equation (2) relates the sum of the scattering and absorption indices from aerosols and molecular components of the atmosphere.

$$\gamma(\lambda) = \alpha_m(\lambda) + \alpha_a(\lambda) + \beta_m(\lambda) + \beta_a(\lambda), \tag{2}$$

$\alpha_m(\lambda)$ and $\alpha_a(\lambda)$ represent the molecular and aerosol absorption coefficients, and $\beta_m(\lambda)$ and $\beta_a(\lambda)$ are the molecular and aerosol scattering coefficients, respectively. Systems are intended to work in the windows of 780–850 and 1520–1600 nm which correspond to atmospheric transmission windows because it is difficult to change the randomness of the atmosphere [17].

The comparison of the particle radius "r" with the wavelength "λ" is used to calculate the scattering attenuation. Rayleigh scattering is predominant when $r < \lambda$ and geometric scattering occurs when $r > \lambda$. When the particle radius is similar to the wavelength ($r \approx \lambda$), the dominant phenomena are Mie scatterings. Table 1 summarizes the relation between particle type, particle radius, and scattering processes [18]. The following is a mathematical representation of the specific attenuation due to scattering:

$$\alpha(\lambda) = \frac{17}{V}\left\{\frac{550}{\lambda}\right\}^{0.195V}, \tag{3}$$

where V is the visibility in km and λ is the wavelength in nm. From (3), it can be observed that the specific attenuation due to scattering is the wavelength-dependent process. Figure 2 is the plot of specific attenuation due to scattering *vs*. visibility for three optical windows.

Table 1
Size and kind of scattering mechanism of various air molecules present in the transmission medium.

Type	**Particle radius (µm)**	**Scattering process**
Air molecules	0.0001	Rayleigh
Haze particle	0.01–1	Rayleigh-Mie
Fog droplet	1–20	Mie-geometrical
Rain	100–10 000	Geometrical
Snow	1000–5000	Geometrical
Hail	5000–50 000	Geometrical

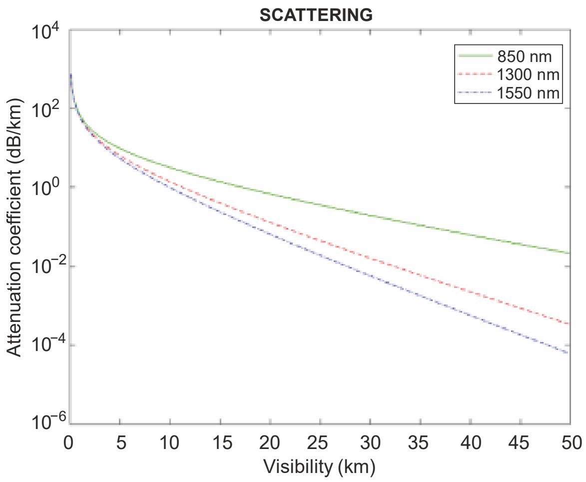

Fig. 2. Specific attenuation due to scattering.

Visibility "V" is an essential parameter that helps relate the severity of the environmental conditions to the actual visual range. Visibility is defined as a distance that a light beam can propagate till the intensity drops by 2% of the original value [19]. The formulae in Table 2 can be used to calculate the specific attenuation owing to fog, rain, and snow. By virtue of the fog particle wavelength being comparable to the propagation wavelength, the attenuation due to fog becomes a paramount contributing factor to the optical signal attenuation [20–23].

2.1. *Atmospheric turbulence models*

On bright sunny days, scintillation affects the performance of many optical wireless communication devices. Scintillation, sometimes known as "hot air", is one of the impacts of temperature differentials on the density of air particles. The air closest to the Earth's surface is warmer than the air at high altitudes due to solar radiation. Warmer air does have a lower density and rises to mix with the cooler air. Eddies are inhomogeneities resulting from the mixing. Eddies are discrete cells of different sizes and temperatures that operate as refractive prisms, creating refractive index variations. This causes random variations in the received signal which drastically impairs the performance of the FSO system, especially over long distances. There are four types of turbulence: faint,

Table 2
Specific attenuation due to weather factors.

Phenomenon	**General techniques**	**Visibility based on relation**
FOG	Mie scattering theory (not the most favourable technique due to involvement of complex computations)	$\beta_{fog}(\lambda) = \frac{3.91}{V}\left(\frac{\lambda}{550}\right)^{-p}$ V (km) is the visibility range, λ (nm) is the operating wavelength, and p is the size distribution coefficient of scattering. Based on the Kim and Kruse models. Figure 3 depicts the specific attenuation caused by fog. According to Kim model, p is given as $p = \begin{cases} 1.6 & V > 50 \\ 1.3 & 6 < V < 150 \\ 0.16V + 0.34 & 1 < V < 6 \\ V - 0.5 & 0.5 < V < 1 \\ 0 & V < 0.5 \end{cases}$ According to Kruse model, p is given as $p = \begin{cases} 1.6 & V > 50 \\ 1.3 & 6 < V < 50 \\ 0.585V^{\frac{1}{3}} & V < 6 \end{cases}$
RAIN	$\beta_{rain} = 1.067R^{0.67}$ in dB/km R (mm/hr): rain rate. Figure 4 shows the specific attenuation due to rain for a specific range of variable rain rates.	$\alpha_{rain} = \frac{2.8}{V}$
SNOW	$\beta_{snow} = aS^b$ in dB/km S (mm/hr) is snow rate and the values of parameters a and b in dry and wet snow are: dry snow – $a = 5.42 \times 10^{-5} + 5.4958776;\ b = 1.38$ wet snow – $a = 1.023 \times 10^{-4} + 3.7855466;\ b = 0.72$	$\alpha_{snow} = \frac{58}{V}$ Figure 5 shows the specific attenuation on account of wet snow and dry snow, respectively.

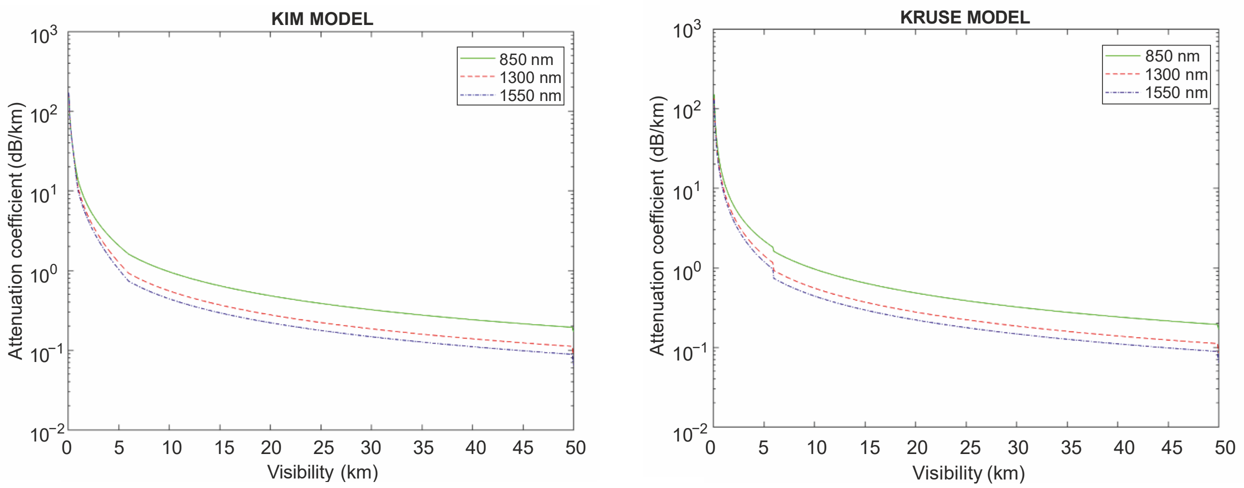

(a) (b)

Fig. 3. Specific attenuation due to fog: Kim model (a) and Kruse model (b).

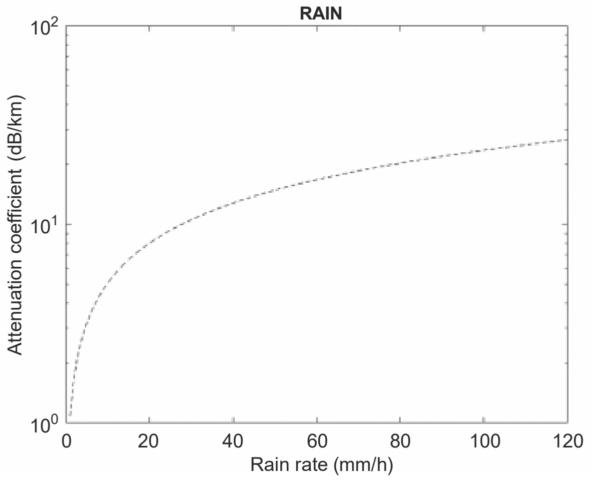

Fig. 4. Specific attenuation due to rain.

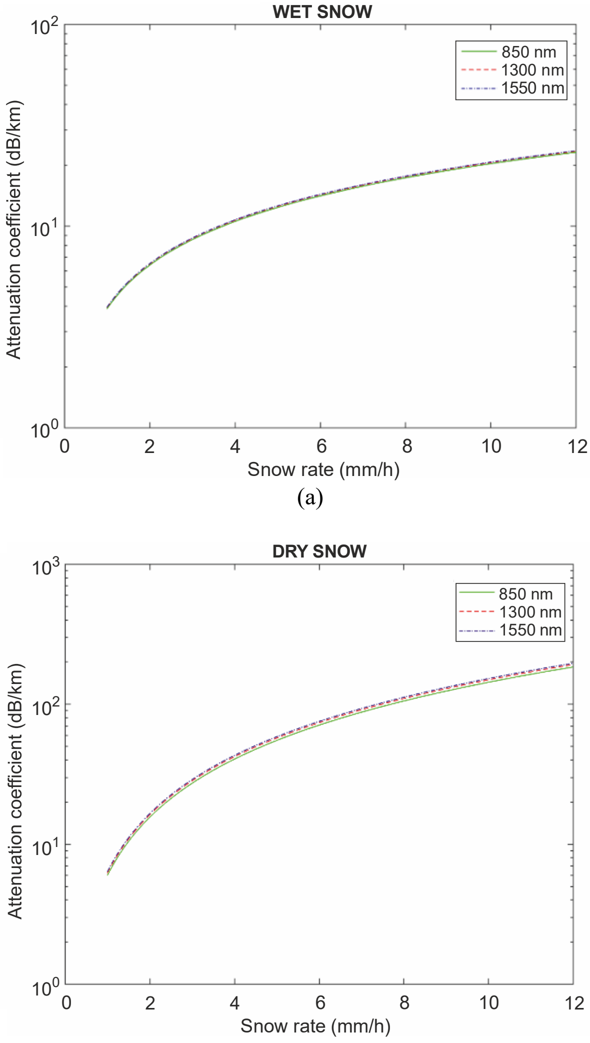

(a)

(b)

Fig. 5. Specific attenuation due to wet snow (a), dry snow (b).

moderate, strong, and saturated. The amplitude of the refractive index shifts, and the distance covered by optical signals through the atmosphere are used to categorize them. Due to the extreme complexity, there is no general model that encompasses all regimes. The three most often reported models for irradiance variation in a turbulent channel are discussed in this work. The weak, weak-to-strong, and saturated regimes are represented by log-normal, gamma–gamma, and negative exponential models, respectively [24].

Kolmogorov proposed the index of the refraction structure parameter C_n^2 to help calculate the amount of refractive index variations: wavelength, altitude, and temperature influence C_n^2. The Hufnagel–Valley (H–V) model is widely used to model C_n^2 in terms of altitude. C_n^2 is mathematically defined as follows:

$$C_n^2(h) = 0.00594\left(\frac{v_w}{27}\right)^2\left(10^{-5}h\right)^{10}\exp\left(\frac{-h}{100}\right) + 2.7\times10^{-16}\exp\left(\frac{-h}{1500}\right) + \hat{A}\exp\left(\frac{-h}{100}\right), \qquad (4)$$

where v_w is the local wind speed perpendicular to the field of travel (the most usually used value is of 21 m/s), $\hat{A}$ is taken as the nominal value of $C_n^2(0)$ at the ground level in $\text{m}^{-2/3}$, and h is the altitude in meters. C_n^2 is assumed to be 1.7×10^{-14} $\text{m}^{-2/3}$ and 8.5×10^{-15} $\text{m}^{-2/3}$ during the day and at night, respectively, near the ground levels. C_n^2 varies between 10^{-12} $\text{m}^{-2/3}$ for heavy turbulence and 10^{-17} $\text{m}^{-2/3}$ for light turbulence, with a standard average value of 10^{-15} $\text{m}^{-2/3}$.

2.1.1. Log-normal channel model

The statistics of irradiance variations in this model follow a log-normal distribution. A single energy dispersive event describes this model which is best suited for mild turbulence environments. The probability density function (PDF) is calculated based on (5):

$$p(I) = \frac{1}{\sqrt{2\pi\sigma_I^2}}\frac{1}{I}\exp(-\frac{\left(\ln\left(\frac{I}{I_0}\right) - E[I]^2\right)}{2\sigma_I^2}, \qquad I \geq 0, \quad (5)$$

where σ_I^2 is the log irradiance for a plane wave, I is the field irradiance and I_0 is the intensity in free space. Depolarization is minimal in severe turbulence conditions. Numerous scatterings caused by turbulent eddies are not accounted by the Rytov approximations. Figure 6 represents the PDF for log-normal distribution for four different variance values.

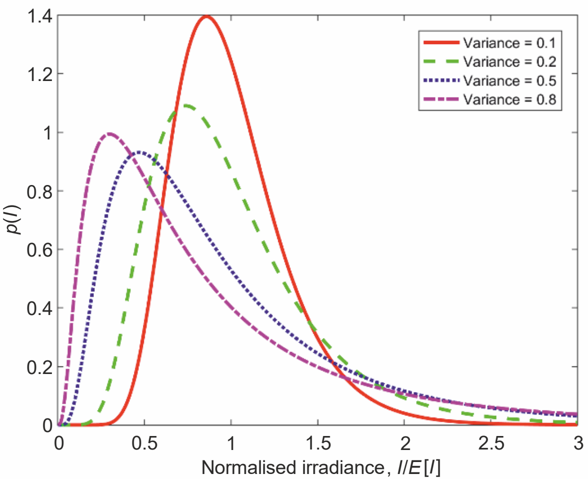

Fig. 6. Log-normal turbulence PDF.

2.1.2. Negative exponential channel model

This model is valid for the saturation regime which has many independent scatterings. The irradiance variation here follows the Rayleigh distribution which has negative exponential statistics. The negative exponential probability density function can be calculated using (6).

$$p(I) = \frac{1}{I_0}\exp\left(-\frac{I}{I_0}\right), \qquad I_0 \geq 0, \tag{6}$$

where $E[I] = I_0$ is the mean received irradiance. Figure 7 represents the PDF distribution for the negative exponential model for different values of field intensity in free space.

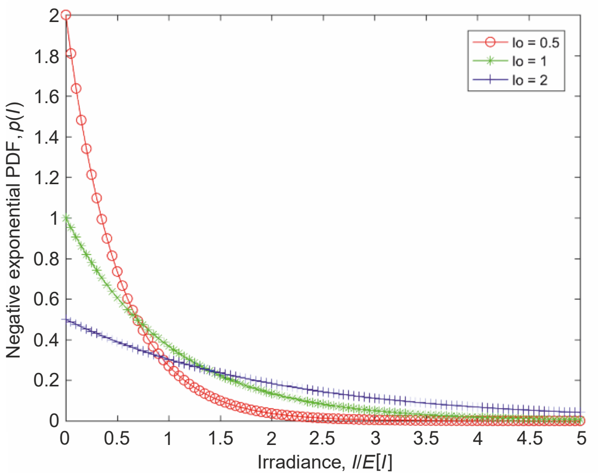

Fig. 7. Negative exponential turbulence PDF.

2.1.3. Gamma–gamma channel model

Both small-scale (scattering) and large-scale (refraction) effects are taken into consideration in this model. This model considers all turbulence regimes, from moderate to strong. For the saturation regime, the model approaches a negative exponential distribution. The gamma–gamma irradiance distribution function is calculated based on (7).

$$p(I) = \frac{2(\alpha\beta)^{(\alpha+\beta)/2}}{\Gamma(\alpha)\Gamma(\beta)} I^{((\alpha+\beta)/2)-1} \mathrm{K}_{\alpha-\beta}\left(\sqrt[2]{\alpha\beta I}\right), I \geq 0, \tag{7}$$

$\mathrm{K}_n(.)$ is the modified Bessel function of the second kind of order n and $\Gamma(.)$ represents the gamma function. The effective number of large- and small-scale eddies in the scattering process is represented by α and β and is related to atmospheric conditions according to (8) and (9).

$$\alpha = \left[\exp\left(\frac{0.49\sigma_I^2}{\left(1+1.11\sigma_I^{12/5}\right)^{7/6}}\right)-1\right]^{-1}, \tag{8}$$

$$\beta = \left[\exp\left(\frac{0.51\sigma_I^2}{\left(1+0.69\sigma_I^{12/5}\right)^{5/6}}\right)-1\right]^{-1}, \tag{9}$$

where σ_I^2 is the Rytov variance. Figure 8 represents the PDF of the gamma–gamma turbulence model for three regimes.

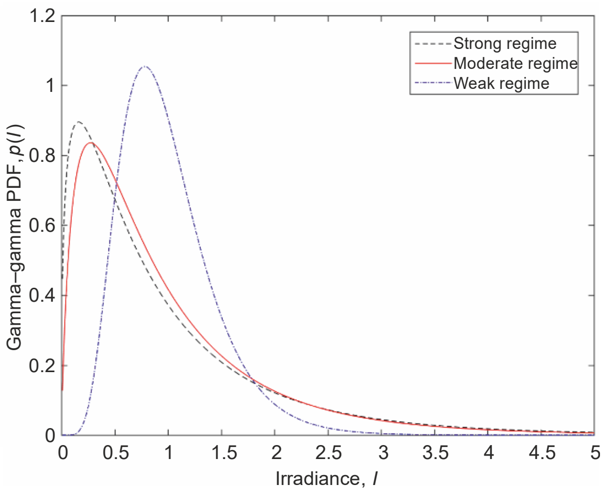

Fig. 8. Gamma–gamma turbulence PDF.

Figure 9 summarizes the relation between scintillation index value and corresponding distributions. The log-normal distribution is famous because of its mathematical simplicity; nonetheless, it is only relevant to the weak turbulence [25, 25]. The negative exponential distribution is applicable only to the saturation regime. Despite its mathematical complexity, the gamma–gamma model, when considered in confinement, covers from caters to a wider scale of the scintillation index. Hence, the gamma–gamma model is considered more comprehensive.

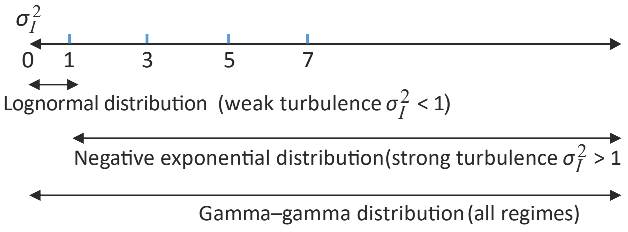

Fig. 9. Irradiance statistics and appropriate distribution summary.

3. Hybrid FSO/mmWave system

There is a trade-off between system availability and link range in commercial FSO systems. The mmWave communication systems, with carrier frequencies ranging from many tens of GHz to more than 100 GHz, provide comparable data speeds to FSO systems. These systems are suited for point-to-point communications across lengths of less than 20 km. This technology limited range allows for the spectrum reuse. While fog affects the performance of FSO lines, rain causes a power loss owing to dispersion in mmWave links because rain drops have diameters equivalent to the mmWave wavelength [27]. Furthermore, absorption maxima in 24 GHz, 60 GHz, and 125 GHz are caused by the oxygen absorption. Near 94 GHz, power absorption becomes minimal, allowing mmWave devices to cover greater distances. As a result, mmWave at this frequency can supplement FSO links, extending the range and availability of the hybrid FSO/mmWave system. Figure 10 summarizes the characteristics of the mmWave channel.

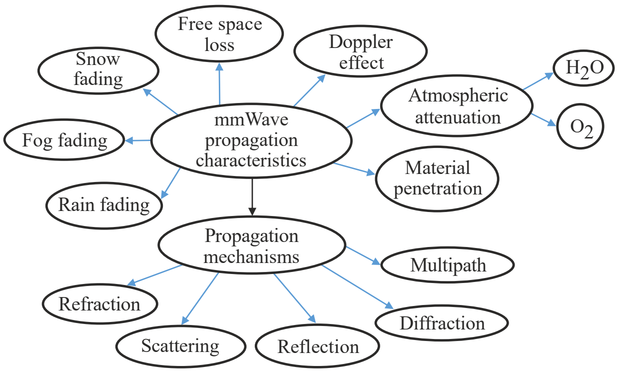

Fig. 10. mmWave channel characteristics.

The general mmWave channel equation is as follows:

$$y(t) = H \times x(t) + n(t), \tag{10}$$

where $y(t)$ is the received signal, H represents the overall channel model parameters, $x(t)$ is the transmitted signal and $n(t)$ is the noise signal. The mmWave channel model is built on a series of nested link attenuation scenarios that calculate margin losses due to rain, fog, atmospheric (water vapour, and oxygen) attenuation, and multipath effects. The formula to calculate the total transmission loss for a link with a frequency higher than10 GHz is given by (11).

$$\begin{aligned}\text{Attenuation (dB)} &= 92.45 + 20 \log f \\ &\quad + 20 \log D + \text{Excess Attenuation}\,,\end{aligned} \tag{11}$$

where f is the frequency in GHz and D is the distance in km. Absorption losses owing to atmospheric gases, attenuation due to fog and mist, attenuation due to rainfall, and multipath effects deriving from surface reflection are all examples of the excessive attenuation. For example, considering 60 GHz as the propagation frequency, overall attenuation varies between 140 dB/km to 180 dB/km for the LoS link [28]. The following is a quick rundown of these key attenuation variables.

3.1. *Gaseous attenuation*

Many gaseous elements in the atmosphere absorb microwave radiation by molecule absorption which occurs when changes in quantum level occur at a certain resonant frequency or a small band of frequencies. Only oxygen and water vapour exhibit visible resonance in the radio wave band in the atmosphere. The oxygen and water vapour attenuation for 60 GHz is estimated to be $\gamma_0 = 14.9$ dB/km and $\gamma_w = 0.1869$ dB/km at a temperature of 20 °C and a water vapour concentration of 7.5 g/m^3 (relative humidity of 42% at 20 °C) [29, 30]. Figure 11 helps describe absorption at 28 GHz, 40 GHz, and 60 GHz, respectively.

3.2. *Effect of fog*

For backup RFs higher than 10 GHz, minuscule fog droplets induce dispersion and considerable attenuation. At frequencies lower than 10 GHz, the effect is insignificant. The Rayleigh approximation is applicable for fog droplets smaller than 0.01 cm and frequencies lower than 200 GHz.

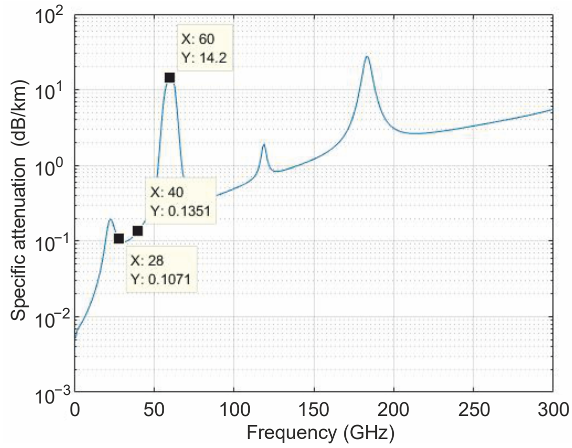

Fig. 11. Specific attenuation due to oxygen and water vapour absorption for mmWave signals.

Attenuation can be described as a total water content per unit volume [31]. The specific attenuation γ_{Fog} is defined as follows:

$$\gamma_{Fog} = K_l M\,, \tag{12}$$

where γ_{Fog} is the specific attenuation in dB/km, K_l is the specific attenuation coefficient (dB/km)/(g/m^3), and M is the liquid water density (g/m^3).

A mathematical model based on Rayleigh scattering may be used to compute the specific attenuation coefficient. For the dielectric permittivity (f) of water, this model uses the double-Debye model, where $\varepsilon(f) = \acute{\varepsilon} + j\ddot{E}$. The specific attenuation coefficient is defined as follows:

$$K_l = \frac{0.819 f}{\ddot{E}(1 + \eta^2)}\,, \tag{13}$$

where f is the frequency in GHz, $\dot{}\ddot{E}$ is the complex dielectric permittivity and η is represented in (14).

$$\eta = \frac{2 + \varepsilon'}{\ddot{E}} \tag{14}$$

The complex dielectric permittivity of water is given in (15).

$$\ddot{E}(f) = \frac{f(\varepsilon_0 - \varepsilon_1)}{f_p\left(1 + \left(\frac{f}{f_p}\right)^2\right)} + \frac{f(\varepsilon_1 - \varepsilon_2)}{f_s\left(1 + \left(\frac{f}{f_s}\right)^2\right)} \tag{15}$$

$$\varepsilon'(f) = \frac{f(\varepsilon_0 - \varepsilon_1)}{f_p\left(1 + \left(\frac{f}{f_p}\right)^2\right)} + \frac{f(\varepsilon_1 - \varepsilon_2)}{f_s\left(1 + \left(\frac{f}{f_s}\right)^2\right)} + \varepsilon_2 \tag{16}$$

In the above expressions, f_p and f_s are the principal and secondary relaxation frequencies in GHz, respectively, and are expressed as

$$f_p = 20.09 - 142\left(\frac{300}{T} - 1\right) + 294\left(\frac{300}{T} - 1\right)^2, \tag{17}$$

$$f_s = 590 - 1500\left(\frac{300}{T} - 1\right). \tag{18}$$

Here, T is the temperature in Kelvin and $\varepsilon_0 = 77.6 - 103.3\left(\frac{300}{T} - 1\right)$, $\varepsilon_1 = 5.48$ and $\varepsilon_2 = 3.1$. Figure 12 depicts the specific attenuation due to fog on mmWave signals for three different frequencies, respectively.

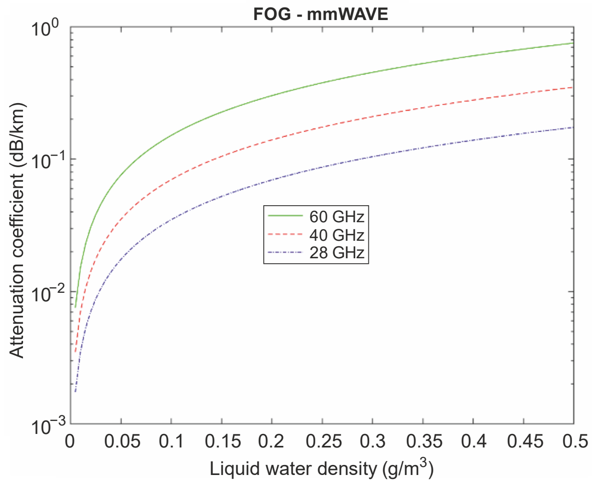

Fig. 12. Attenuation due to fog for mmWave signals.

3.3. *Effect of rain*

The association between specific attenuation and rain rate is given in (19).

$$\gamma_{rain} = kR^{\alpha}. \tag{19}$$

The Crane model specifies the values of the constants k and α for various frequencies. The ITU-R terrestrial model and the Crane model are two prominent methods for estimating rain attenuation [32, 33]. Constants k and α depend upon the frequency and microstructure of rain and can be mathematically defined as follows:

$$k = \frac{(k_H + k_V + (k_H - k_V)\cos^2\theta\cos 2T)}{2} \tag{20}$$

$$\alpha = \frac{k_H\alpha_H + k_V\alpha_V + (k_H\alpha_H - k_V\alpha_V)\cos^2\theta\cos 2T}{2k} \tag{21}$$

The values of constants k_H, k_V, α_H, and α_V are given in Refs. 32 and 33. Figure 13 depicts the specific attenuation due to rain on mmWave signals for three different frequencies.

3.4. *Effect of snow*

The actual structure of snowflakes makes it challenging to analyse radio wave attenuation, as there are many weather-dependent variations in type, morphology, dielectric constants, and size distribution [34]. In the case of snow, the specific attenuation in terms of snow rate S is represented by (22).

$$\gamma_{snow} = 0.00349\frac{S^{1.4}}{\lambda^4} + 0.0024\frac{S}{\lambda}. \tag{22}$$

Figure 14 depicts the specific attenuation due to snow on mmWave signals for three different frequencies.

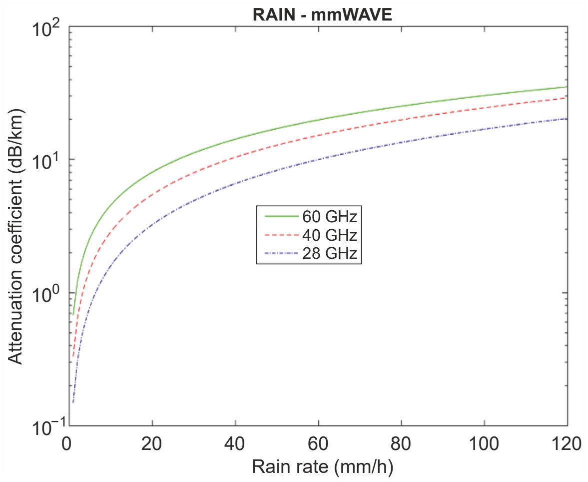

Fig. 13. Attenuation due to rain for mmWave signals.

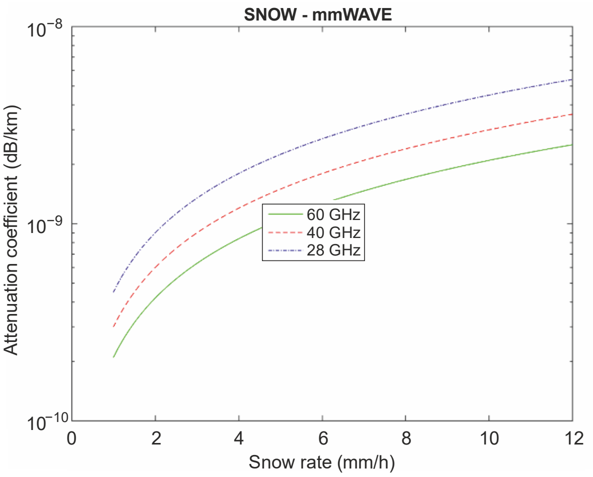

Fig. 14. Attenuation due to snow for mmWave signals.

It can be observed that the specific attenuation due to rain is typically from 1 dB/km to 42 dB/km for mmWave links. Attenuation due to O_2 absorption is typically at 60 GHz. Figure 15 is a comparison of oxygen attenuation with specific attenuation due to rain at 60 GHz. Specific attenuation due to fog for FSO links ranges from 0.7 dB/km to 170 dB/km. Based on the above results, it can be concluded that rain is the largest contributor to the signal attenuation for the mmWave link, whereas fog has the

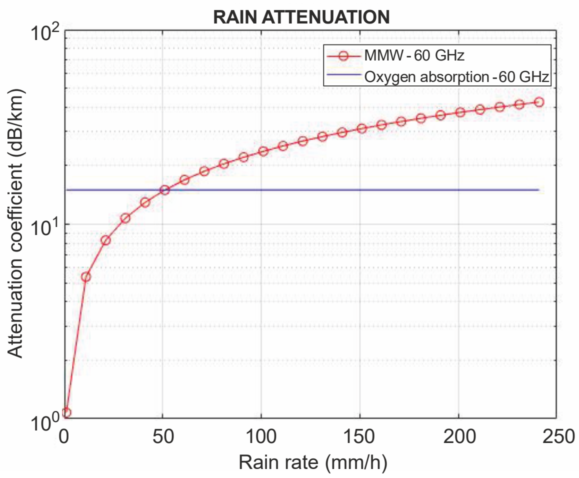

Fig. 15. Comparison of attenuation due to rain at oxygen absorption at 60 GHz for mmWave signals.

highest impact on the signal in the FSO channel. This complimentary behaviour of both technologies helps overcome their individual drawbacks. The FSO link, due to its high bandwidth capabilities, is an ideal choice to be a primary link. Both links have similar traits in terms of offered data rates. A combined FSO/mmWave link ensures that the wireless communication link is more stable and able. The complete operation of a hybrid link is influenced by visibility which depends on atmospheric conditions. Based on channel status information, like signal strength, the user needs to be able to switch between two sources. The next section describes an efficient switching mechanism which ensures improved link availability in adverse weather conditions.

4. Switching techniques

By using mmWave link along with FSO, the link availability to match commercial carrier standards can be essentially guaranteed [35]. However, during the active time of the primary FSO link, the available bandwidth of the mmWave link is wasted. In order to effectively utilize the available bandwidth, a switch-over technique has been discussed for the hybrid system. Under default conditions, whilst the FSO system is operational, the mmWave link is being used to transport more data allowing the system total capacity to be better utilized. A predefined threshold value is used to monitor the signal level at the receiver (P_R). When the signal strength received on the FSO link falls below this threshold (α_{FSO}), the system switches to the mmWave link. After the switch-over, data is transmitted on the mmWave link and the FSO link is used to carry test data. The received signal strength of the FSO is continuously checked and compared until it exceeds a specific higher threshold, indicating that it has recovered and that load sharing on two independent data streams can resume. Correspondingly, despite the loss of the FSO link due to heavy fog, the system remains operational at all times. When the mmWave link fails, the same method is used to avoid pendulum switching by evaluating the intensity of the signal received by the mmWave link against a higher threshold. When both channels are unavailable, test data are transmitted on both of links to see if one of them restores. The switching criterion is adaptively altered to ensure that from the initiation to the complete switch-over it occurs prior to the collapse of the FSO or mmWave link. The receiver readily acknowledges all packets and transmits information to the transmitter on both paths if it detects malformed packets or a low threshold level. If the transmitter discovers a link failure based on a threshold value or retransmission request, the packet next to the last acknowledged packet by the receiver is transmitted on the functional link, whilst test data is sent on the failed link. Since the connection between the two communication devices is still the same, both sides will sense the threshold at the same time. Receiver packet transmission request based on exceeding a specific allowed bit error rate (BER) is an additional check for a connection failure, enabling this system to become a fool proof setup. Handshaking is performed between both ends to share channel availability information and information on the last received data packet. After both links regain operational status, then both links resume load sharing. The logical block diagram and technical overview of the envisaged switch-over algorithm between FSO and mmWave links are shown in Figs. 16 and 17. The suggested switch-over approach considerably improves bandwidth usage by leveraging the growing ubiquity of load sharing during the timeframe when both links are active, which accounts for more than 90% of the total observed time. This minimizes bandwidth inefficiency from 100% to less than 10% of the total measured time.

5. Conclusions

For the last mile dilemma, FSO can provide an effective ultra-high bandwidth solution. Due to its ability to provide high data rate, FSO has great potential to grow out from a niche market. This study examines the approach core strengths and shortcomings, highlighting current state-of-the-art advancements and essential design characteristics. The channel model for both technologies considers all dominant attenuation contributors such as rain, fog, gaseous attenuation, etc. In this paper, the hybrid FSO/mmWave system as an effective solution has been discussed. The authors focused on examining the

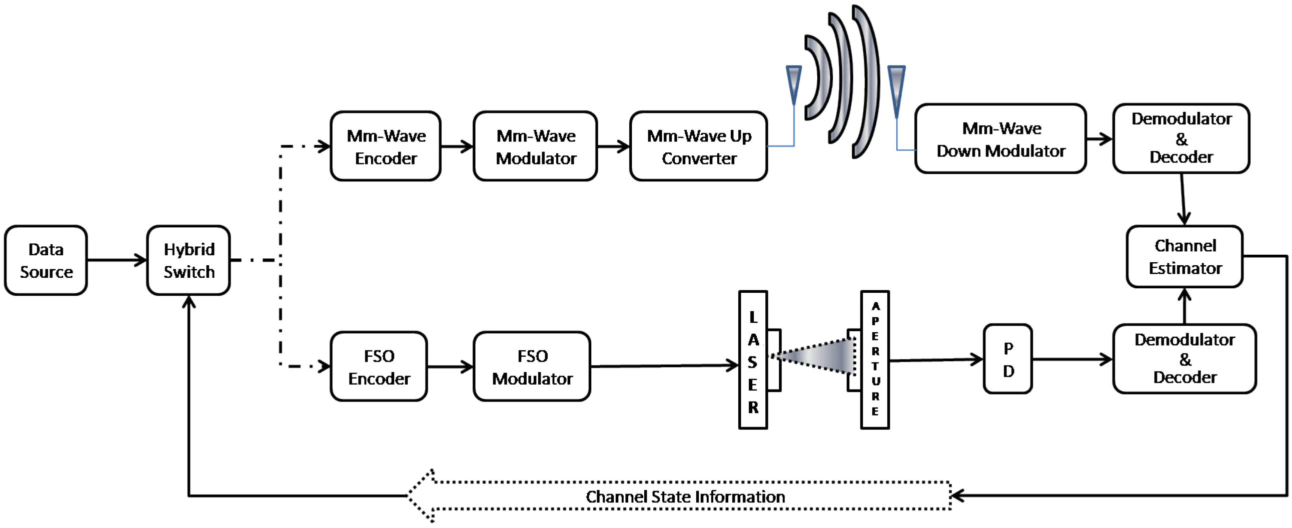

Fig. 16. Proposed hybrid system block diagram.

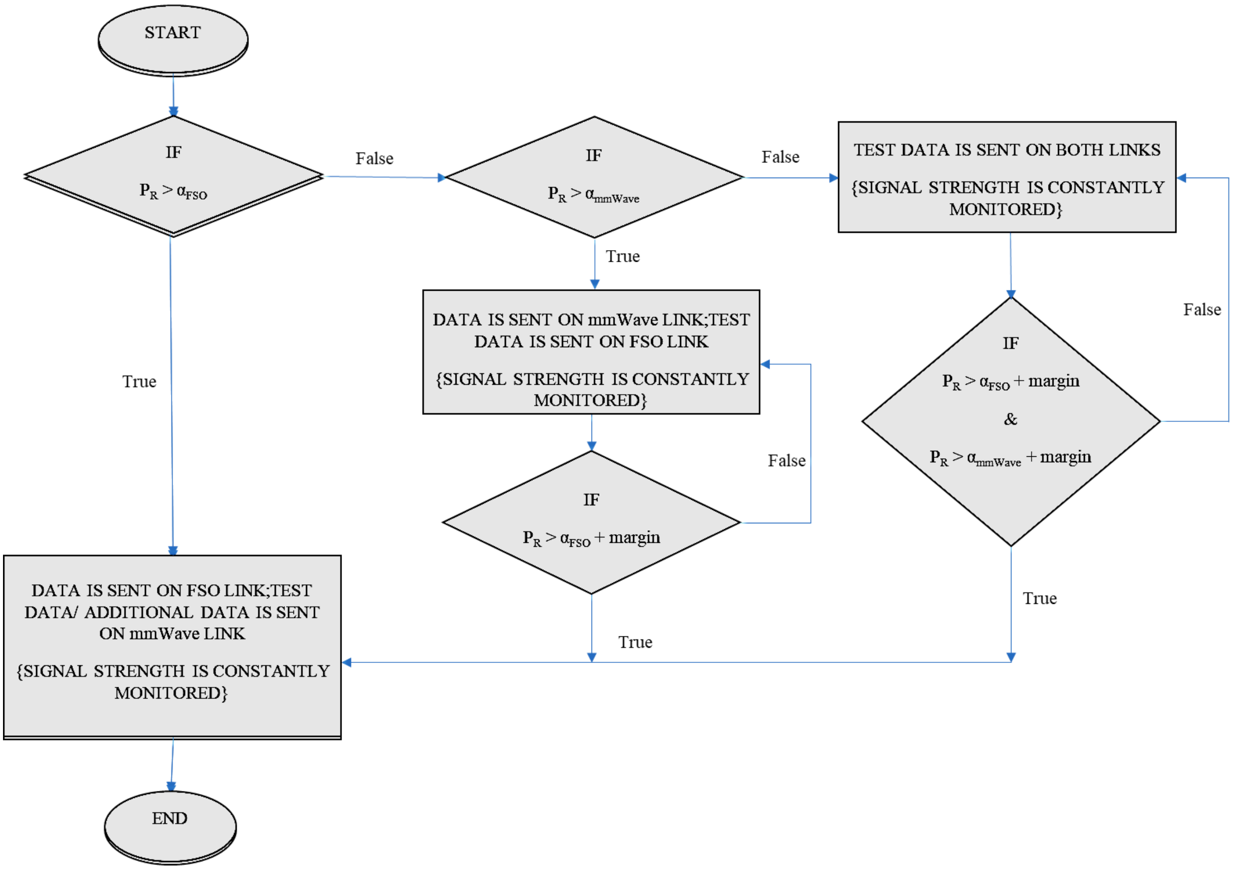

Fig. 17. Proposed switch-over algorithm.

availability of the hybrid FSO/mmWave link. The proposed hybrid architecture can greatly extend the percentage of link availability, thus ensuring that the conditions for carrier-class commercial deployment are met.

A hybrid FSO/mmWave system has been presented as a manner to facilitate high-bandwidth point-to-point connectivity over extended distances in the access network. A novel switch-over algorithm allows for a better bandwidth utilization while ensuring link availability at all times.

Authors' statement

This project was conceived by all authors. Research concept and design, data analysis and interpretation, writing the article and final approval of the article were done by I. Lakshmi Priya. All the simulations were carried out by Isanaka Lakshmi Priya. M. Meenakshi was involved in data analysis and interpretation, writing the article, final approval of the content and constructive modification of the article. All authors read and approved the final manuscript.

References

[1] Chowdhury, M. Z., Hasan, M. K., Shahjalal, M., Hossan, M. T. & Jang, Y. M. Optical wireless hybrid networks: trends, opportunities, challenges, and research directions. *IEEE Commun. Surv. Tutor.* **22**, 930–966 (2020). https://doi.org10.1109/COMST.2020.2966855

[2] Liu, G. & Jiang, D. 5G: Vision and requirements for mobile communication system towards year 2020. *Chinese J. Eng.* 2016, 1–8 (2016). https://doi.org/10.1155/2016/5974586

[3] Ford, R. *et al.* Achieving ultra-low latency in 5G millimeter wave cellular networks. *IEEE Commun. Mag.* **55**, 196–203 (2017). https://doi.org/10.1109/MCOM.2017.1600407CM

[4] Tunc, C., Ozkoc, M. F., Fund, F. & Panwar, S. S. The blind side: latency challenges in millimeter wave networks for connected vehicle applications. *IEEE Trans. Veh. Technol.* **70**, 529–542 (2021). https://doi.org/10.1109/TVT.2020.3046501

[5] Mikolajczyk, J. *et al.* Optical wireless communications operated at long-wave infrared radiation. *Int. J. Electron. Telecommun.* **66**, 383–387 (2020). https://doi.org/10.24425/ijet.2020.131889

[6] Mikołajczyk, J. *et al.* Analysis of free-space optics development. *Metrol. Meas. Syst.* **24**, 653–674 (2017). https://doi.org/10.1515/mms-2017-0060

[7] Son, I. K. & Mao, S. A survey of free space optical networks ☆. *Digit. Commun. Netw.* **3**, 67–77 (2017). https://doi.org/10.1016/j.dcan.2016.11.002

[8] Khalighi, M. A. & Uysal, M. Survey on free space optical communication: a communication theory perspective. *IEEE Commun. Surv. Tutor.* **16**, 2231–2258 (2014). https://doi.org/10.1109/COMST.2014.2329501

[9] Rockwell, D. A. & Mecherle, G. S. Wavelength selection for optical wireless communications systems. *Proc. SPIE* **4530**, 26–35 (2001). https://doi.org/10.1117/12.449812

[10] Bloom, S., Korevaar, E., Schuster, J. & Willebrand, H. Understanding the performance of free-space optics. *J. Opt. Netw.* **2**, 178–200 (2003). https://doi.org/10.1364/JON.2.000178

[11] Willebrand, H. & Ghuman, B. S. *Free Space Optics: Enabling Optical Connectivity In Today's Networks*. (Indianapolis, Indiana: SAMS, 2002).

[12] Jeyaseelan, J., Sriram Kumar, D. & Caroline, B. E. Disaster management using free space optical communication system. *Photonic Netw. Commun.* **39**, 1–14 (2020). https://doi.org/10.1007/s11107-019-00865-9

[13] Anandkumar, D. & Sangeetha, R. G. A survey on performance enhancement in free space optical communication system through channel models and modulation techniques. *Opt. Quantum Electron.* **53**, 5 (2020). https://doi.org/10.1007/s11082-020-02629-6

[14] Siegel, T. & Chen, S.-P. Investigations of free space optical communications under real-world atmospheric conditions. *Wirel. Pers. Commun.* **116**, 475–490 (2021). https://doi.org/10.1007/s11277-020-07724-1

[15] Kaur, S. Analysis of inter-satellite free-space optical link performance considering different system parameters. *Opto-Electron. Rev.* **27**, 10–13 (2019). https://doi.org/10.1016/j.opelre.2018.11.002

[16] Shah, D., Joshi, H. & Kothari, D. Comparative BER analysis of free space optical system using wavelength diversity over exponentiated weibull channel. *Int. J. Electron. Telecommun.* **67**, 665–672 (2021). https://doi.org/10.24425/ijet.2021.137860

[17] Ghassemlooy, Z. & Popoola, W. O. Terrestrial Free-Space Optical Communications. in *Mobile and Wireless Communications* (eds. Fares, S. A. & Adachi, F.) 355–392 (IntechOpen, 2010). https://doi.org/10.5772/7698

[18] Ricklin, J. C., Hammel, S. M., Eaton, F. D. & Lachinova, S. L. Atmospheric Channel Effects on Free-Space Laser Communication. in *Optical and Fiber Communication Reports*: *Free-Space Laser Communications* (eds. Majumdar, A. K. & Ricklin, J. C.) 9–56 (Springer, 2006). https://doi.org/10.1007/978-0-387-28677-8_2

[19] Ghassemlooy, Z., Popoola, W. & Rajbhandari, S. *Optical Wireless Communications: System and Channel Modelling with Matlab®.* (CRC press, 2019).

[20] Kim, I. I., McArthur, B. & Korevaar, E. J. Comparison of Laser Beam Propagation at 785 Nm And 1550 Nm In Fog And Haze For Optical Wireless Communications. in *Optical Wireless Communications, Proc. SPIE* **4214**, 26–37 (2001). https://doi.org/10.1117/12.417512

[21] Al Naboulsi, M. C. Sizun, H. & de Fornel, F. Fog attenuation prediction for optical and infrared waves. *Opt. Eng.* **43**, 319–329 (2004). https://doi.org/10.1117/1.1637611

[22] Brown, R. G. W. Optical channels. Fibres, clouds, water and the atmosphere. *J. Mod. Opt.* **36**, 552 (1989). https://doi.org/10.1080/09500348914550651

[23] Sree Madhuri, A., Immadi, G. & Venkata Narayana, M. Estimation of effect of fog on terrestrial free space optical communication link. *Wirel. Pers. Commun.* **112**, 1229–1241 (2020). https:/doi.org/10.1007/s11277-020-07098-4

[24] Friedlander, S. K. & Topper, L. *Turbulence: Classic Papers on Statistical Theory*. (Interscience Publishers, 1961).

[25] Kolmogorov, A. N. The local structure of turbulence in incompressible viscous fluid for very large Reynolds numbers. *Proc. R. Soc. A* **434**, 9–13 (1991). https://doi.org/10.1098/rspa.1991.0075

[26] Zhu, X. & Kahn, J. M. Free-space optical communication through atmospheric turbulence channels. *IEEE Trans. Commun.* **50**, 1293–1300 (2002). https://doi.org/10.1109/TCOMM.2002.800829

[27] Dat, P. T. *et al.* A Study on Transmission of RF Signals over a Turbulent Free Space Optical Link. in *2008 IEEE Int. Topical Meeting on Microwave Photonics jointly held with 2008 Asia-Pacific Microwave Photonics Conf.* 173–176 (2008) https://doi.org/10.1109/MWP.2008.4666664

[28] Makarov, D. S., Tretyakov, M. Y. & Rosenkranz, P. W. Revision of the 60-GHz atmospheric oxygen absorption band models for practical use. *J. Quant. Spectrosc. Radiat. Transf.* **243**, 106798 (2020). https://doi.org/10.1016/j.jqsrt.2019.106798

[29] He, Q., Li, J., Wang, Z. & Zhang, L. Comparative study of the 60 GHz and 118 GHz oxygen absorption bands for sounding sea surface barometric pressure. *Remote Sens.* **14**, 2260 (2022). https://doi.org/10.3390/rs14092260

[30] Arvas, M. & Alsunaidi, M. Analysis of Oxygen Absorption at 60 GHz Frequency Band. in *2019 IEEE International Symposium on Antennas and Propagation and USNC-URSI Radio Science Meeting Proc.* 2127–2128 (2019) https://doi.org/10.1109/APUSNCURSINRSM.2019.8888884

[31] ITU-R Recomendation. *Attenuation Due to Clouds and Fog* https://www.itu.int/rec/R-REC-P.840-3-199910-S/en (1999).

[32] Crane, R. K. A *Two-Component Rain Model For the Prediction of Attenuation and Diversity Improvement* https://ntrs.nasa.gov/api/citations/19820025716/downloads/19820025716.pdf (1982).

[33] ITU-R Recomendation. *Recommendation Itu-R P.838-1 Specific Attenuation Model for Rain for Use in Prediction Methods* https://www.itu.int/dms_pubrec/itu-r/rec/p/R-REC-P.838-1-199910-S!!PDF-E.pdf (1999).

[34] Amarasinghe, Y., Zhang, W., Zhang, R., Mittleman, D. M. & Ma, J. Scattering of terahertz waves by snow. *J. Infrared Millim. Terahertz Waves* **41**, 215–224 (2020). https://doi.org/10.1007/s10762-019-00647-4

[35] Davis, C. C., Smolyaninov, I. I. & Milner, S. D. Flexible optical wireless links and networks. *IEEE Commun. Mag.* **41**, 51–57 (2003). https://doi.org/10.1109/MCOM.2003.1186545